Electronic Supplementary Material (ESI) for RSC Advances.

Selective Zn^{2+} sensing using a modified bipyridine complex

Mahesh Akula, Patrick El Khoury, Amit Nag* and Anupam Bhattacharya*

Birla Institute of Technology and Science-Pilani(Hyderabad Campus), Hyderabad-500078, Andhra Pradesh, India

e-mail: anupam@hyderabad.bits-pilani.ac.in. amitnag@hyderabad.bits-pilani.ac.in.

SUPPORTING INFORMATION

Contents:

Materials and methods: All starting materials were purchased from Aldrich, Spectrochem, SRL, and SdFine(India) and used directly without further purification. Solvents were dried using standard methods and distilled before use. Visualization on TLC was achieved by use of UV light (254 nm) or iodine. ^{1}H NMR (300MHz and 400 MHz) and ^{13}C (75 MHz and 100MHz) spectra were recorded in $CDCl_3$ and DMSO solution with TMS as internal standard. The mass spectrum was recorded on Agilent 1100/LC MSD Trap SL version. Column chromatography was performed on silica gel (100–200 mesh, SRL. India).

Scheme and procedure for preparation of ligands

Scheme-1: Synthesis of 4-(pyridine-2-yl)-3*H*-pyrrolo[2,3-*c*]quinoline

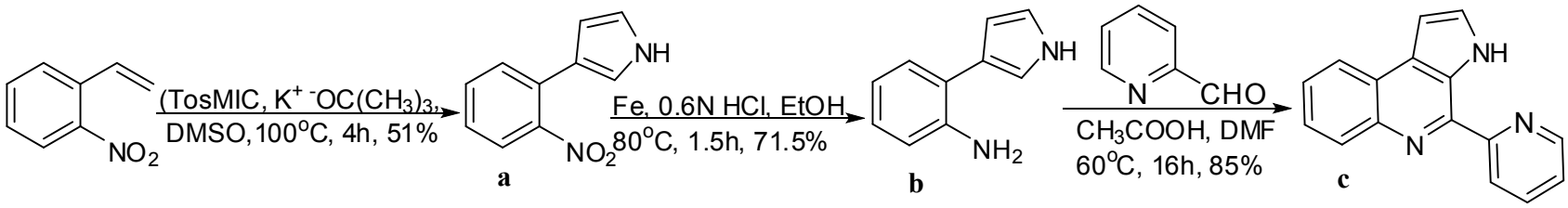

Procedure:

Synthesis of *o*-nitrophenylpyrrole (a): To a solution of *o*-nitrostyrene (2.4 g, 16.091 mmol)**(2)** in DMSO(30 ml), TosMIC(4 g, 20.5 mmol) and *t*-BuOK (3.611 g, 32.2 mmol) were added, and the reaction mixture was stirred for 4h at 100 ^{0}C. After completion of the reaction as indicated by TLC, brine solution (30 ml) was added to reaction mixture and it was extracted with ethyl acetate (3 x 50 ml), the combined organic layer was dried over anhydrous Na_2SO_4. Ethyl acetate was removed under vacuum. The crude product was subjected to column chromatography (Silica gel, 8-10% EtOAc-Hexane) to provide the pure compound as a yellow coloured liquid. Yield: 1.52 g, 51%

Structure confirmed by ^{1}H,^{13}C NMR and mass spectrum and was found consistent with those described in the literature [1].

Synthesis of *o*-aminophenylpyrrole (b): To a solution of *o*-nitrophenylpyrrole (1.3 g, 6.914 mmol) in ethanol (20 ml), Fe(3.858 g, 69.082 mmol) and 0.6N HCl (1.5 ml), were added and the reaction mixture was stirred at 60 ^{0}C for 4h.The reaction mixture was cooled to room temperature and passed through celite pad and the solvent was evaporated. HCl was neutralized with $NaHCO_3$ and aqueous solution was extracted with EtOAc (3 x 50 ml), the combined organic layer was washed with brine (2x20ml) and dried over

Na_2SO_4. Ethyl acetate was removed under vacuum. Crude product thus obtained was subjected to column chromatography (Silica gel, 30-40% EtOAc-Hexane) to afford the desired compound as a brown liquid. Yield: 0.780 g, 71.5%

Structure confirmed by ^1H,^{13}C NMR and mass spectrum and was found consistent with those described in the literature [1].

Synthesis of 4-(pyridine-2-yl)-3*H*-pyrrolo[2,3-*c*]quinoline (c): To a solution of aminophenylpyrrole (298 mg, 1.89 mmol) and pyridine-2-carboxaldehyde (202 mg, 1.89 mmol) in DMF (15 ml), was added acetic acid (20 mol%). The solution was stirred for 12 hours at 60 ^oC. After completion of reaction as indicated by TLC, the reaction mixture was cooled to room temperature. Brine (10 ml), $NaHCO_3$ (5 ml) were added to the reaction mixture and it was extracted with ethyl acetate (3x 30 ml). The combined organic layer was washed with brine (30 ml) and dried over sodium sulfate. Removal of ethyl acetate under reduced pressure gave the crude product, which was chromatographed over silica gel to afford the desired compound **c** as yellow solid. Yield: 393 mg, 85%. Melting point: 155 ^oC.

Structure confirmed by ^1H,^{13}C NMR and mass spectrum and was found consistent with those described in the literature [2].

Scheme-2: Synthesis of 4-(pyridine-2-yl)-3*H*-furo[2,3-*c*]quinoline and 4-(pyridine-2-yl)-3*H*-thieno[2,3-*c*]quinoline

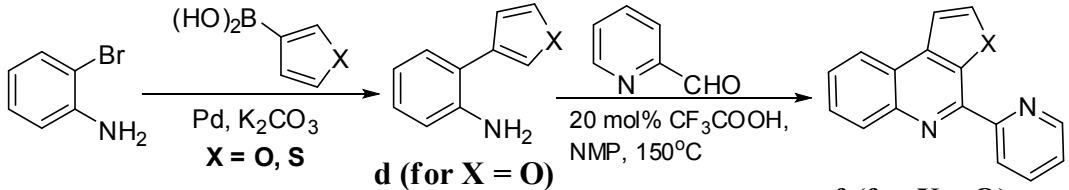

Procedure:

Synthesis of 2-(furan-3-yl)aniline (d):

DMF (5ml) was taken in a round bottom flask and kept under nitrogen atmosphere. 2-iodoaniline (200 mg, 0.91mmol), furan-3-boronic acid (122 mg, 1.09 mmol) and Cs_2CO_3 (600 mg, 1.8 mmol) were subsequently added to it and the reaction mixture was stirred for 5 minutes. Afterwards, $Pd(PPh_3)_4$ (210 mg, 20 mol%) was added and the reaction mixture was heated at 100 ^oC for 7hr. After completion of reaction as indicated by TLC, reaction mixture was diluted with water and extracted with EtOAc (3 x 10 ml).The

organic layer was washed with brine solution and dried over anhydrous Na_2SO_4. Crude product obtained was subjected to column chromatography (Silica gel, 10% EtOAc-Hexane) to afford the compound as brown oil. Yield: 143 mg (98 %).

^{1}H NMR (400 MHz, $CDCl_3$) δ 3.83 (s, 2H), 6.63 (dd, *J* = 1.8, 0.9 Hz, 1H), 6.73 – 6.82 (m, 2H), 7.09 – 7.14 (m, 1H), 7.20 (dd, *J* = 7.6, 1.5 Hz, 1H), 7.51 (t, *J* = 1.7 Hz, 1H), 7.65 (dd, *J* = 1.4, 0.9 Hz, 1H).

Synthesis of 2-(thiophen-3-yl)aniline (e):

DMF (5ml) was taken in a round bottom flask and kept under nitrogen atmosphere. 2-iodoaniline (400 mg, 1.82 mmol), 3-thienyl boronic acid (280 mg, 2.2 mmol) and Cs_2CO_3 (1.2 gm, 3.6 mmol) were subsequently added to it and the reaction mixture was stirred for 5 minutes. Afterwards, $Pd(PPh_3)_4$ (422 mg, 20 mol%) was added and the reaction mixture was heated at 100 ^{o}C for 10hr. After completion of reaction as indicated by TLC, reaction mixture was diluted with water and extracted with EtOAc (3 x 10 ml).The organic layer was washed with brine solution and dried over anhydrous Na_2SO_4. Crude product obtained was subjected to column chromatography (Silica gel, 10% EtOAc-Hexane) to afford the compound as yellow oil. Yield: 274 mg (85.9 %).

Synthesis of 4-(pyridin-2-yl)furo[2,3-*c*]quinoline (f):

140 mg (0.88 mmol) of 2-(furan-3-yl)aniline was dissolved in 3ml of 5% CF_3COOH in NMP, 94 mg (0.88 mmol) of pyridine-2-carboxyladehyde was added to it. Reaction mixture was stirred at 100 ^{o}C for 12h. On completion of the reaction, it was neutralized with saturated $NaHCO_3$ solution. Neutralized solution was extracted with EtOAc (3 x 10ml), organic layer was dried over anhydrous Na_2SO_4 and then evaporated under vacuum. Crude compound was subjected to column chromatography to afford the compound as light yellow solid. Yield: 153 mg (70 %).

^{1}H-NMR (400MHz, DMSO): δ = 7.59 (ddd, *J* = 7.5, 4.8, 1.1 Hz, 1H), 7.73 – 7.83 (m, 3H), 8.08 (td, *J* = 7.8, 1.8 Hz, 1H), 8.22 – 8.26 (m, 1H), 8.45 – 8.49 (m, 2H), 8.85 (dd, *J* = 4.7, 0.7 Hz, 1H) ppm; ^{13}C NMR (101 MHz, DMSO): δ = 106.2, 123.7, 124.4, 124.9, 127.6, 128.5, 130.1, 132.2, 137.5, 143.6, 143.65, 147.05, 149.6, 149.7, 155.2 ppm; IR(KBr): ῡ =3,091, 1,581, 1,352, 1,063, 746 cm^{-1}; ESI-MS: MH^+= 247.

Synthesis of 4-(pyridin-2-yl)thieno[2,3-*c*]quinoline (g):

100 mg (0.57 mmol) of 2-(thiophen-3-yl)aniline was dissolved in 3ml of 5% CF_3COOH in NMP and 68 mg (0.63mmol) of pyridine-2-carboxyladehyde was added to it. Reaction mixture was stirred at 100 ^{o}C for 16h. On completion of the reaction, it was neutralized

with saturated $NaHCO_3$ solution. Neutralized solution was extracted with EtOAc (3 x 10ml), organic layer was dried over anhydrous Na_2SO_4 and then evaporated under vacuum. Crude compound was subjected to column chromatography to afford the compound as white solid. Yield: 75 mg (45 %).

^{1}H-NMR (400MHz, DMSO): δ = 7.63 (ddd, *J* = 7.4, 4.8, 1.0 Hz, 1H), 7.74 – 7.86 (m, 2H), 8.12 (td, *J* = 7.8, 1.7 Hz, 1H), 8.25 – 8.30 (m, 1H), 8.37 (q, *J* = 5.5 Hz, 2H), 8.63 (dd, *J* = 8.1, 1.1 Hz, 1H), 8.84 (d, *J* = 8.0 Hz, 1H), 8.89 (dd, *J* = 4.3, 1.1 Hz, 1H) ppm; ^{13}C NMR (101 MHz, DMSO): δ =121.6, 122.2, 124.3, 124.5, 125.3, 127.8, 128.9, 129.1, 130.0, 137.4, 137.9, 143.9, 144.1, 148.6, 149.8, 155.1 ppm; IR(KBr): ῡ =3,058, 2,925, 1,468, 965, 729 cm^{-1}; ESI-MS: MH^+= 263.

Scheme-3: Synthesis of 3-methyl-4-(pyridin-2-yl)-3*H*-pyrrolo[2,3-*c*]quinoline (h)

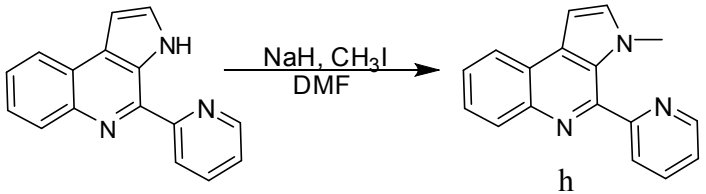

h

60% NaH (32 mg, 1.33 mmol) was taken in a round bottom flask and 3ml of anhydrous DMF was added to it; reaction flask was maintained at 0 ^{o}C under nitrogen atmosphere. 100 mg (0.40 mmol) of 4-(pyridin-2-yl)-3H-pyrrolo[2,3-*c*]quinoline dissolved in DMF was subsequently added and reaction mixture was stirred for 30 min. Afterwards 30 µl (0.48 mmol) of methyl iodide was added and reaction mixture was stirred overnight at room temperature. After completion of the reaction, cold water (10 ml) was poured in the reaction mixture and it was extracted with EtOAc (3 x 10ml). Organic layer was then dried over anhydrous Na_2SO_4 and evaporated under vacuum. Crude compound hence obtained was subjected to column chromatography, which afforded 90 mg (86% yield) of pure 3-methyl-4-(pyridin-2-yl)-3H-pyrrolo[2,3-*c*]quinoline as white solid.

^{1}H NMR (400 MHz, DMSO) δ 3.53 (s, 3H), 7.24 (d, *J* = 2.9 Hz, 1H), 7.54 – 7.66 (m, 4H), 7.93 (d, *J* = 7.8 Hz, 1H), 8.01 – 8.08 (m, 2H), 8.33 – 8.39 (m, 1H), 8.75 (d, *J* = 4.3 Hz, 1H); ESI-MS: MH^+= 260.

S1: ^{1}H NMR(400 MHz, $CDCl_3$) for <u>2-(furan-3-yl)aniline (d)</u>

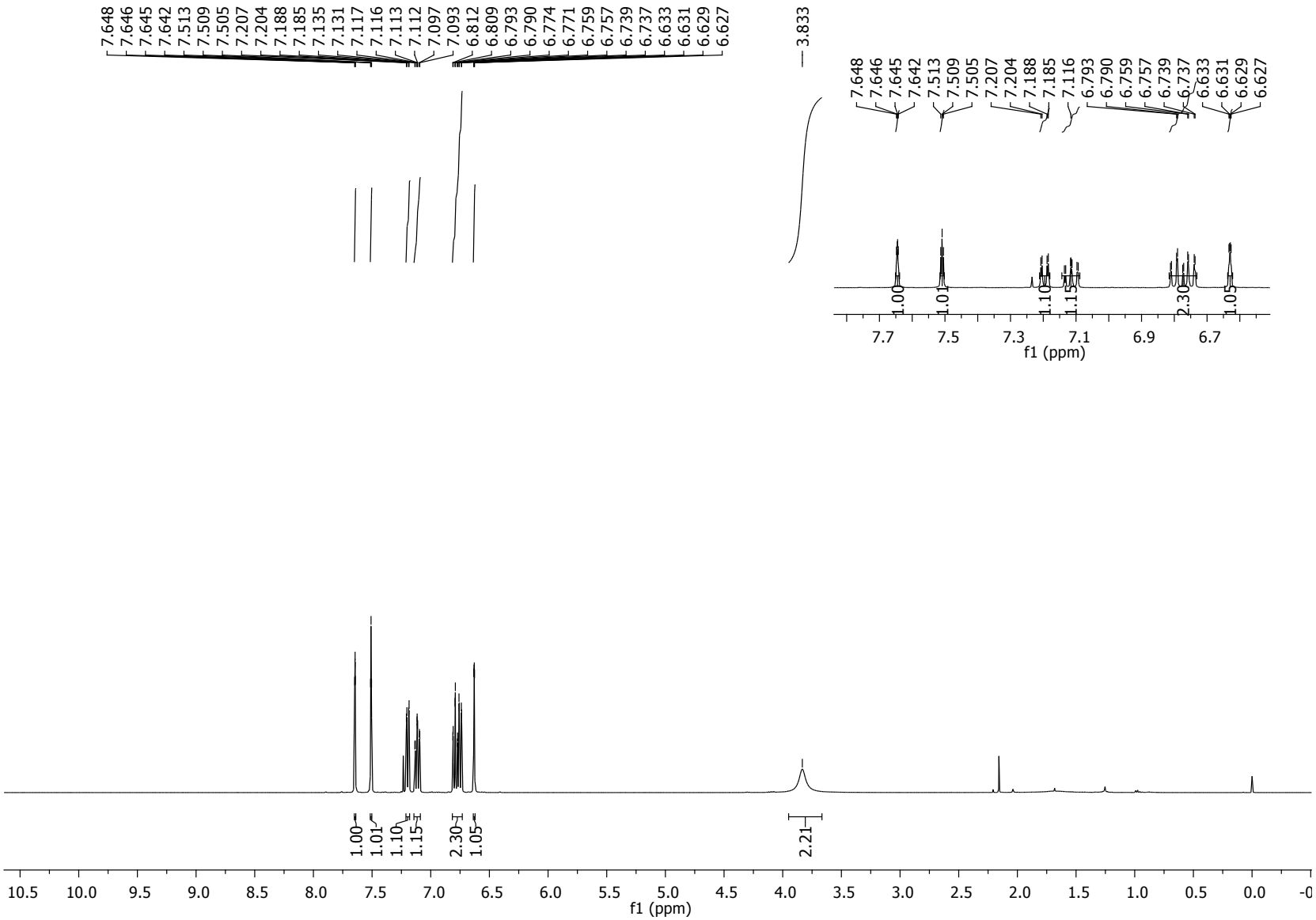

S2: ^{1}H NMR(400 MHz, DMSO-d_6) for <u>4-(pyridin-2-yl)furo[2,3-*c*]quinoline (f)</u>

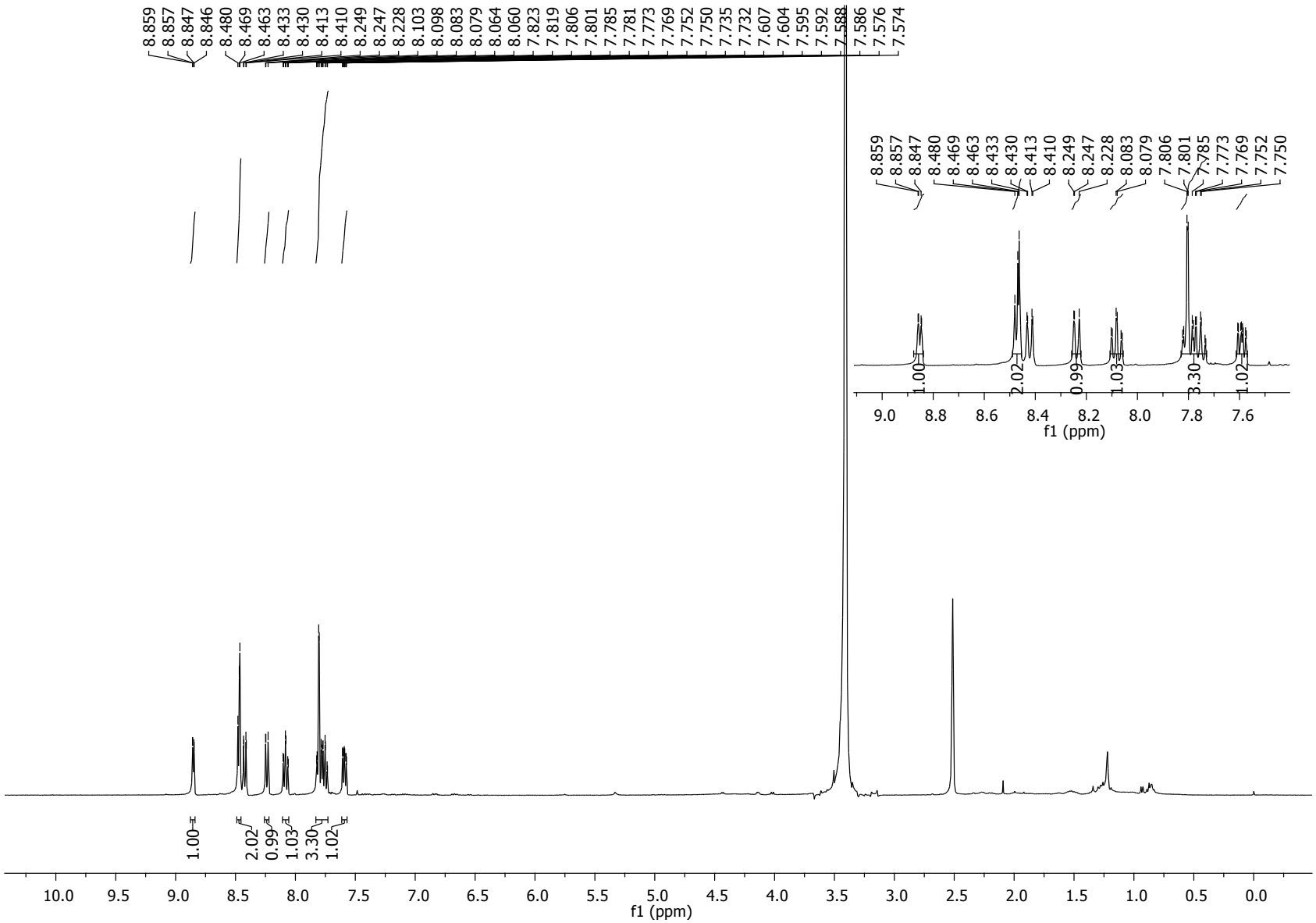

S3: ^{13}C NMR(101 MHz, DMSO-d$_6$) for <u>4-(pyridin-2-yl)furo[2,3-*c*]quinoline (f)</u>

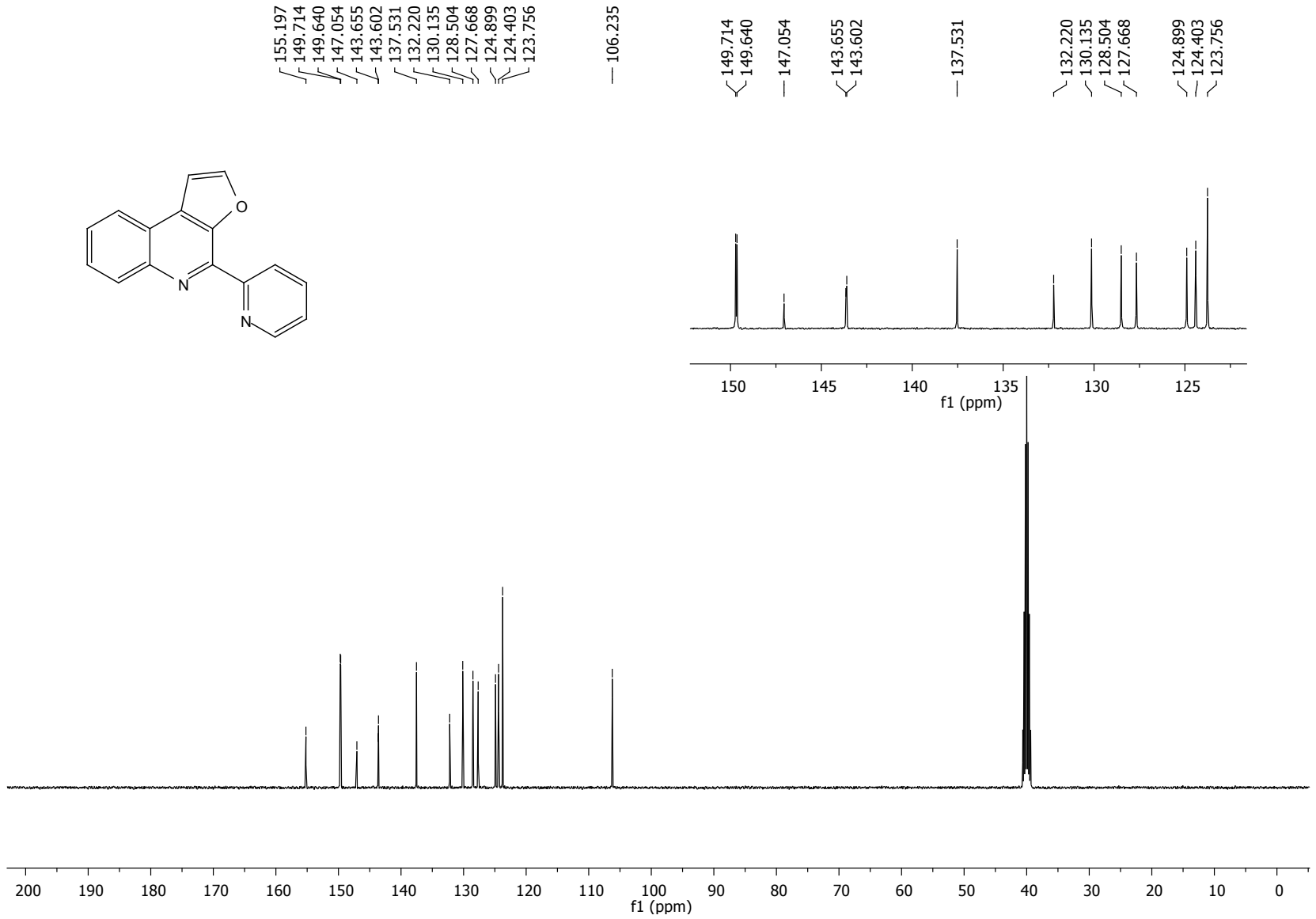

S4: ^{1}H NMR(400 MHz, DMSO-d$_6$) for <u>4-(pyridin-2-yl)thieno[2,3-*c*]quinoline (g)</u>

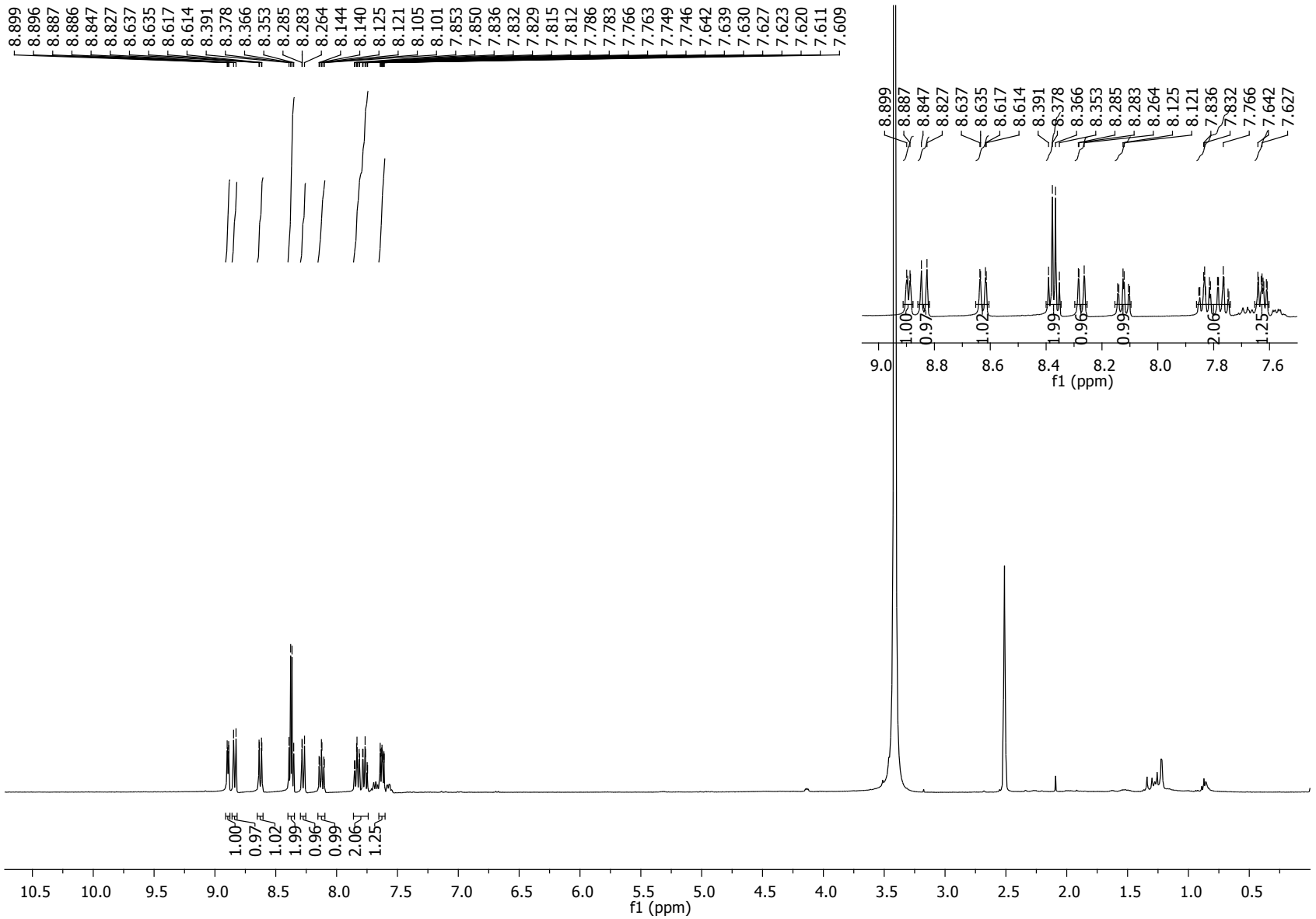

S5: ^{13}C NMR(101 MHz, DMSO-d$_6$) for 4-(pyridin-2-yl)thieno[2,3-*c*]quinoline (g)

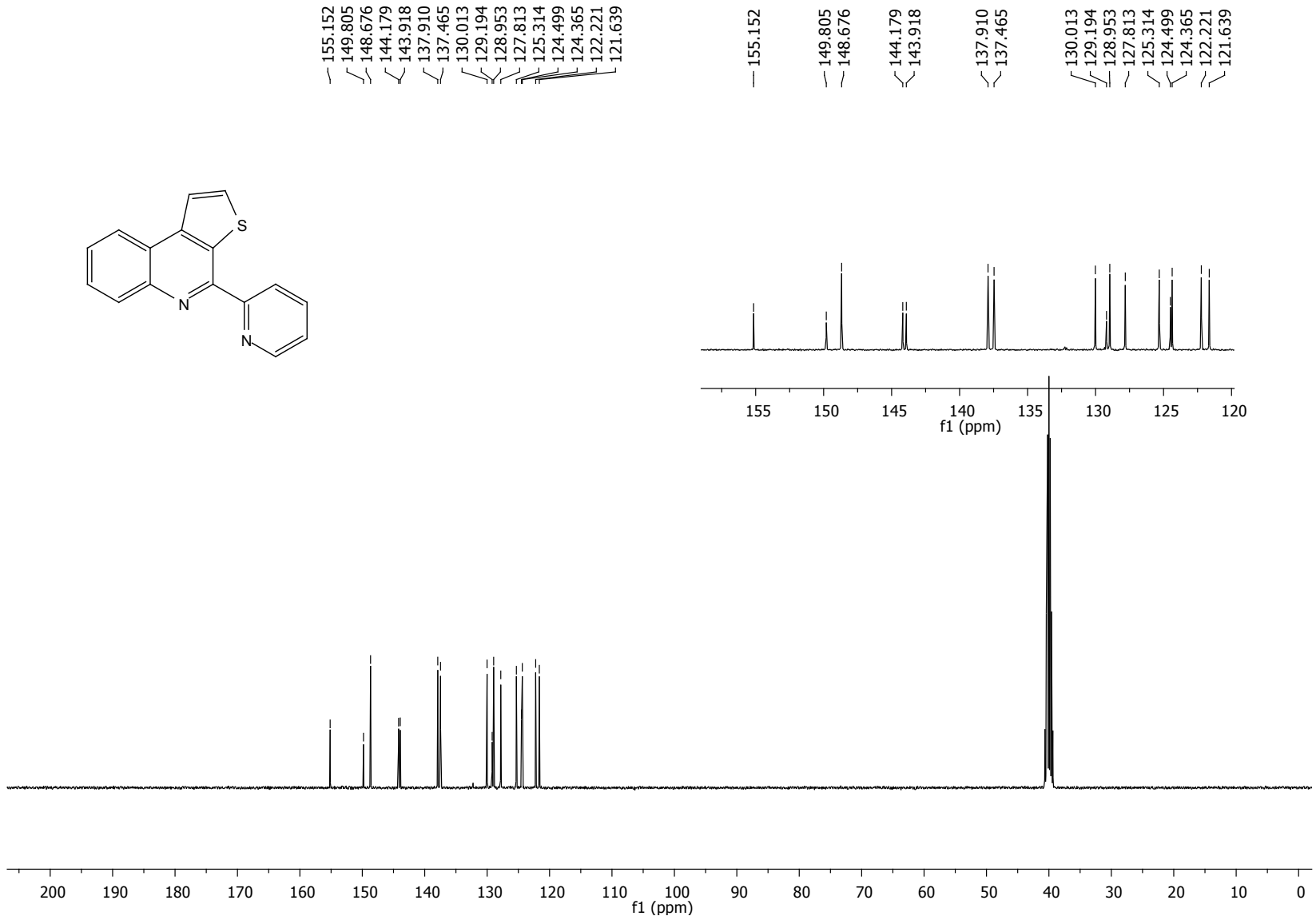

S6: ^{1}H NMR(400 MHz, DMSO-d$_6$) for 3-methyl-4-(pyridin-2-yl)-3*H*-pyrrolo[2,3-*c*]quinoline (h)

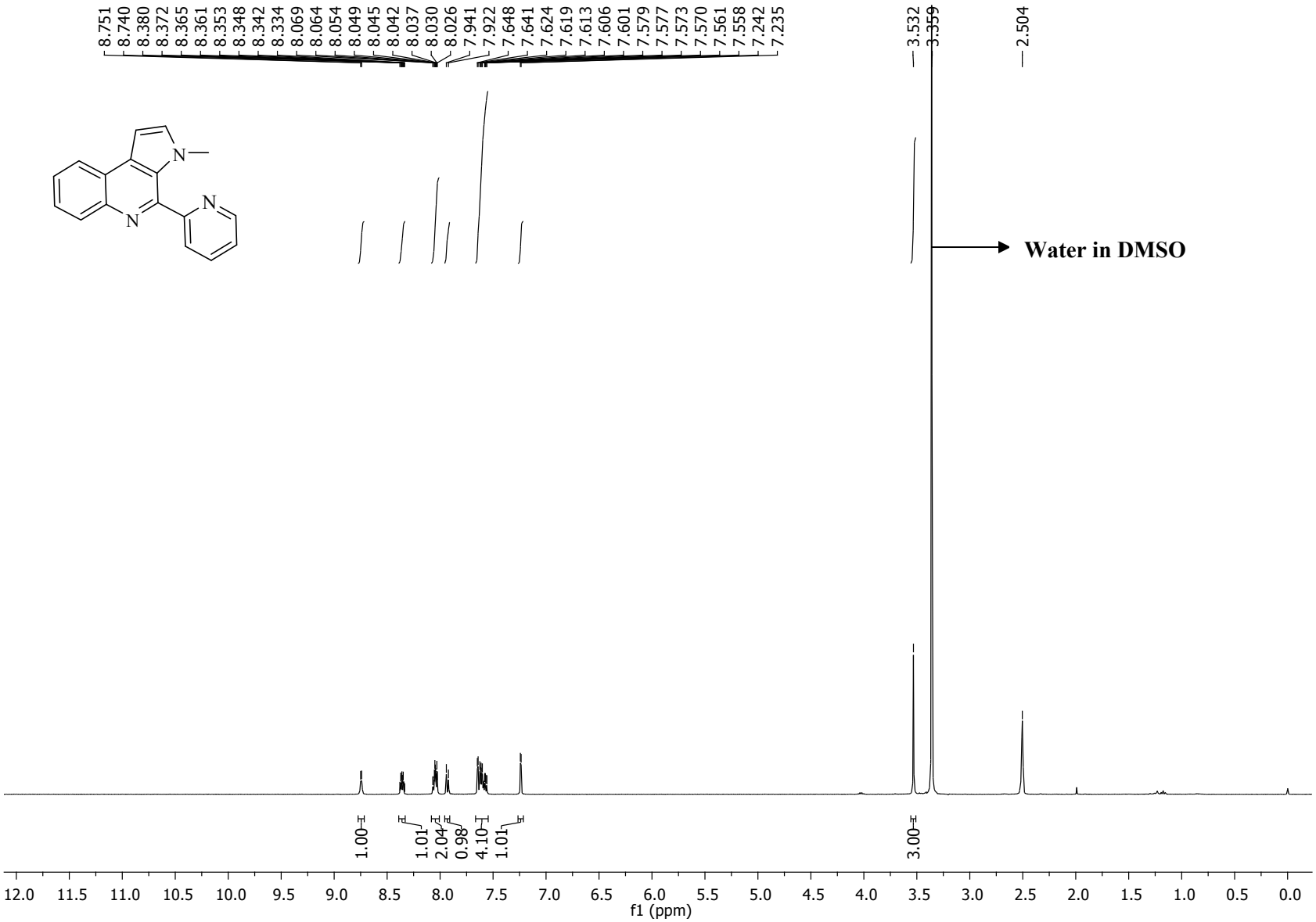

S7: MALDI of the complex(Matrix DHB)

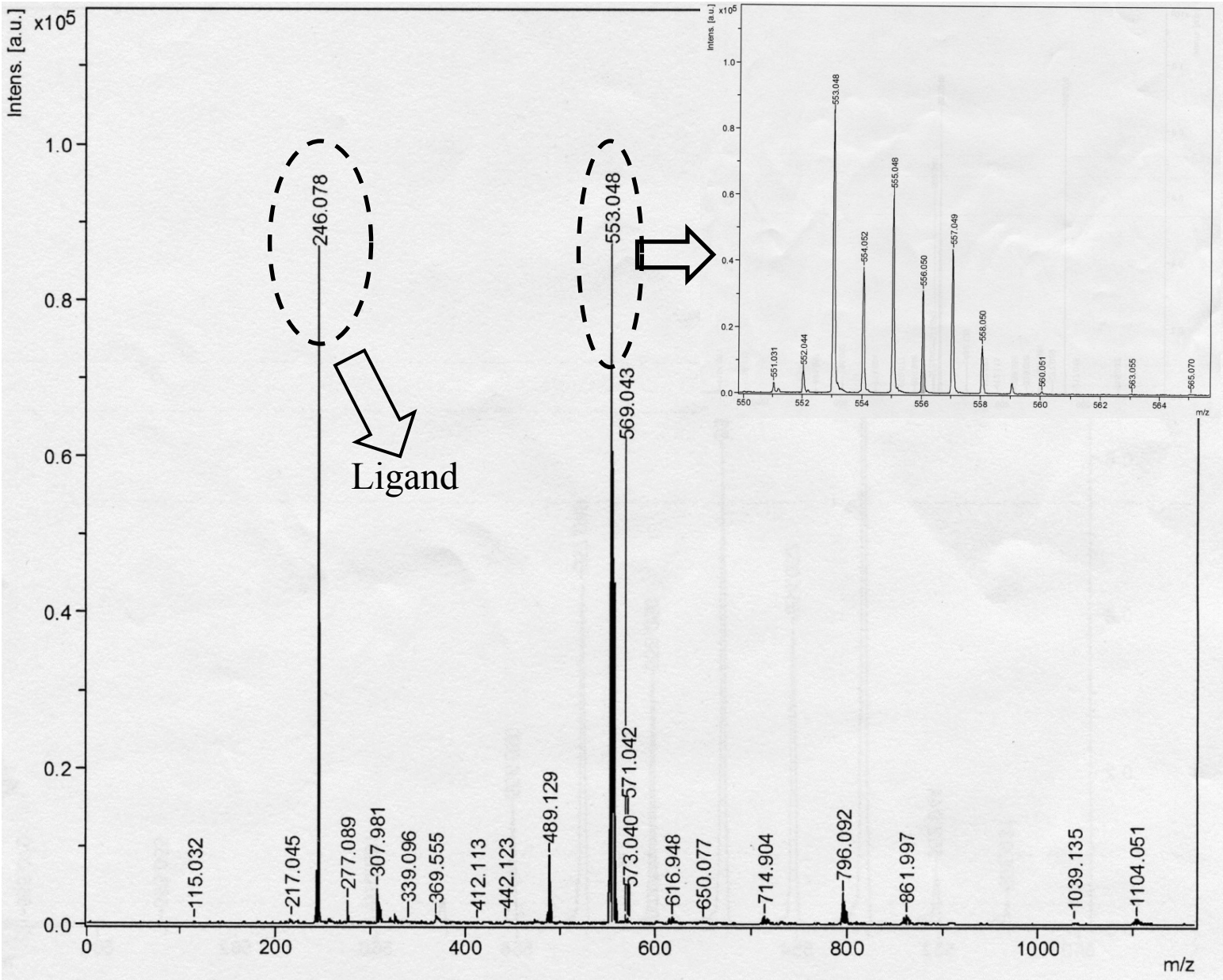

S8: Reversibility experiment

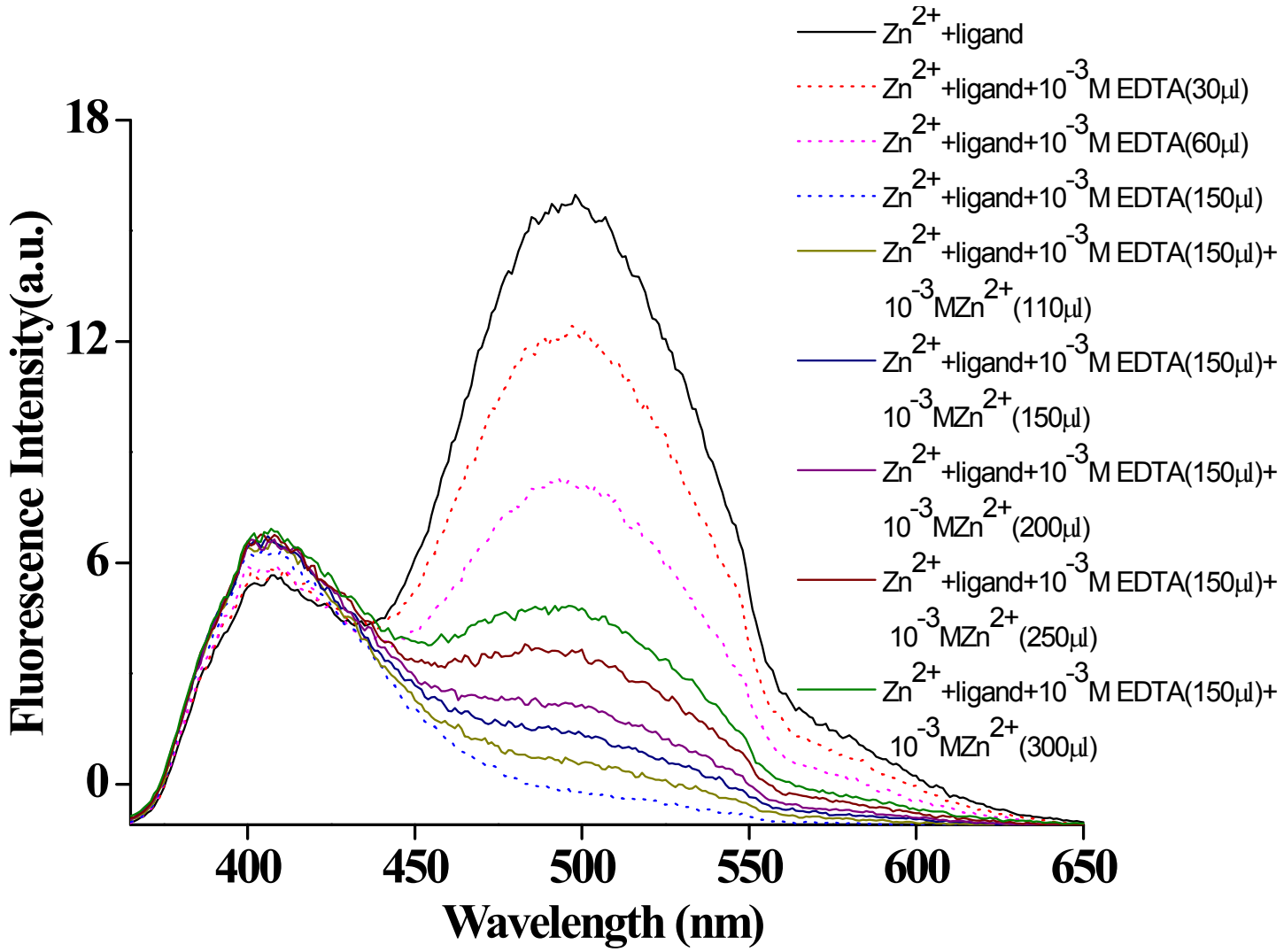

S9: Fluorescence titration

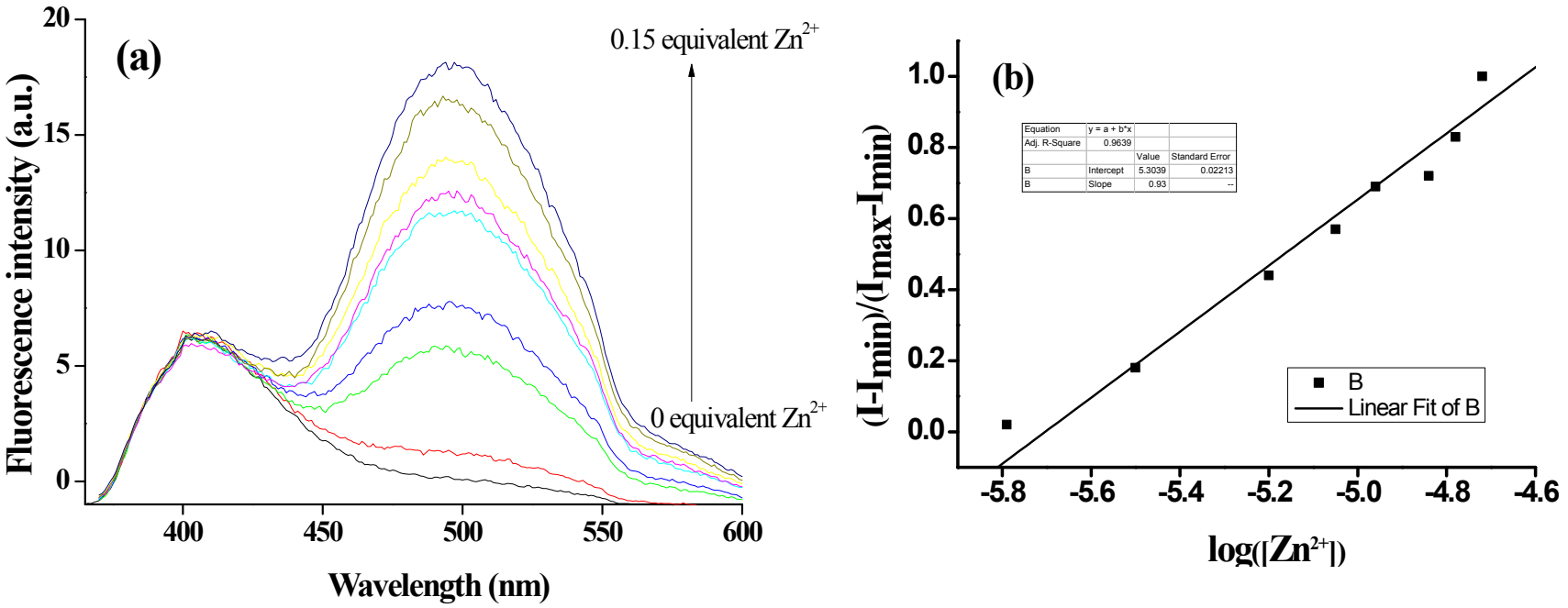

(a) Fluorescence changes during the titration of PPQ (10^{-4} M) with Zn^{2+} (0 - 0.15 equivalent) in DMF. (b) A plot of $(I-I_{min}) / (I_{max}-I_{min})$ vs $\log([Zn^{2+}])$, the calculated detection limit of sensor PPQ is 1.5×10^{-6} M.

S10: pH titration

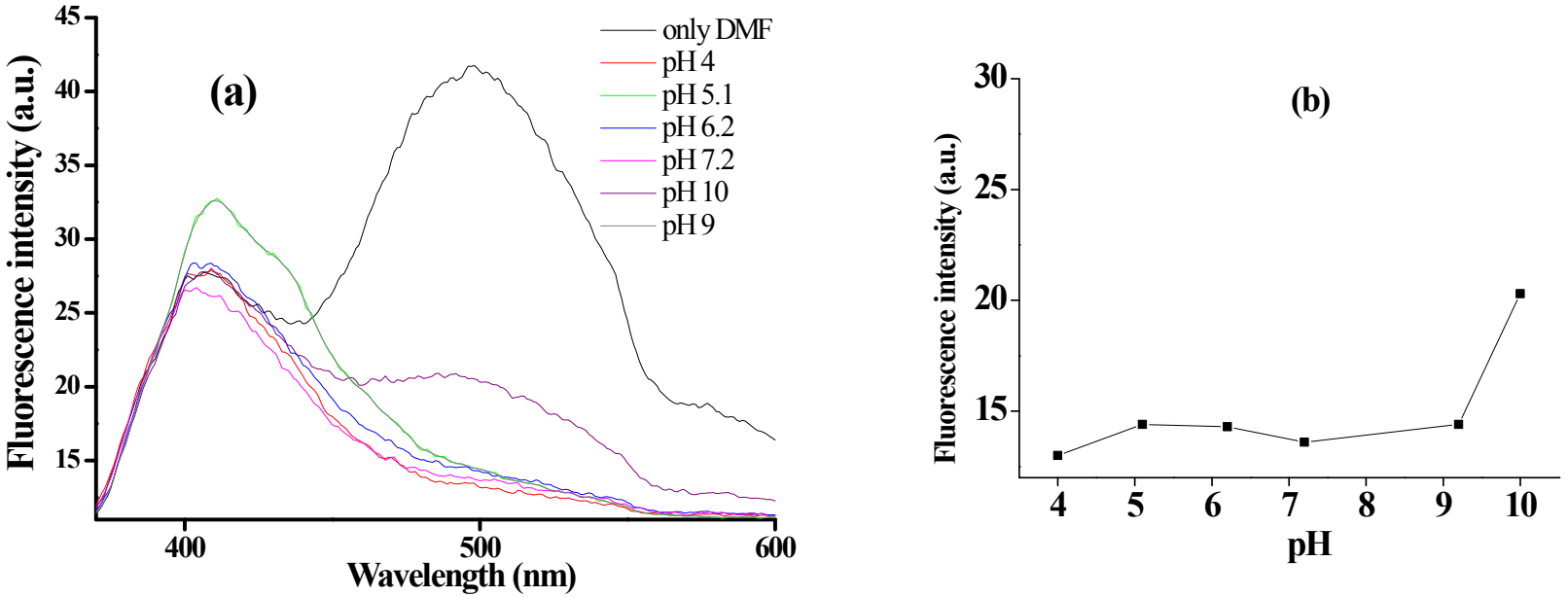

(a) Fluorescence changes during the titration of PPQ (10^{-4} M) with Zn^{2+}(0.15 equivalent) in DMF at different pH mediums. (b) The effect of pH on PPQ (10^{-4} M) with Zn^{2+}(0.15 equivalent).

S11: Ratiometric sensing of PPQ

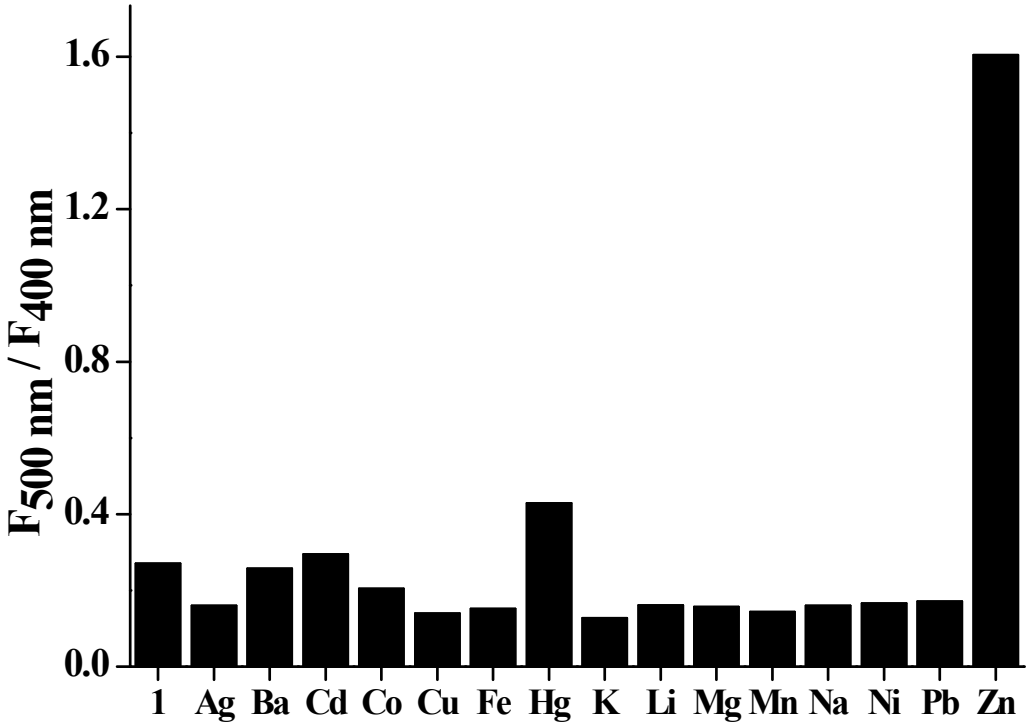

Fluorescence intensity ratio ($F_{500\ nm}/F_{400\ nm}$) of PPQ in the presence of various metal ions.

S12: MALDI of the complex formed with Co^{2+} (Matrix DHB)

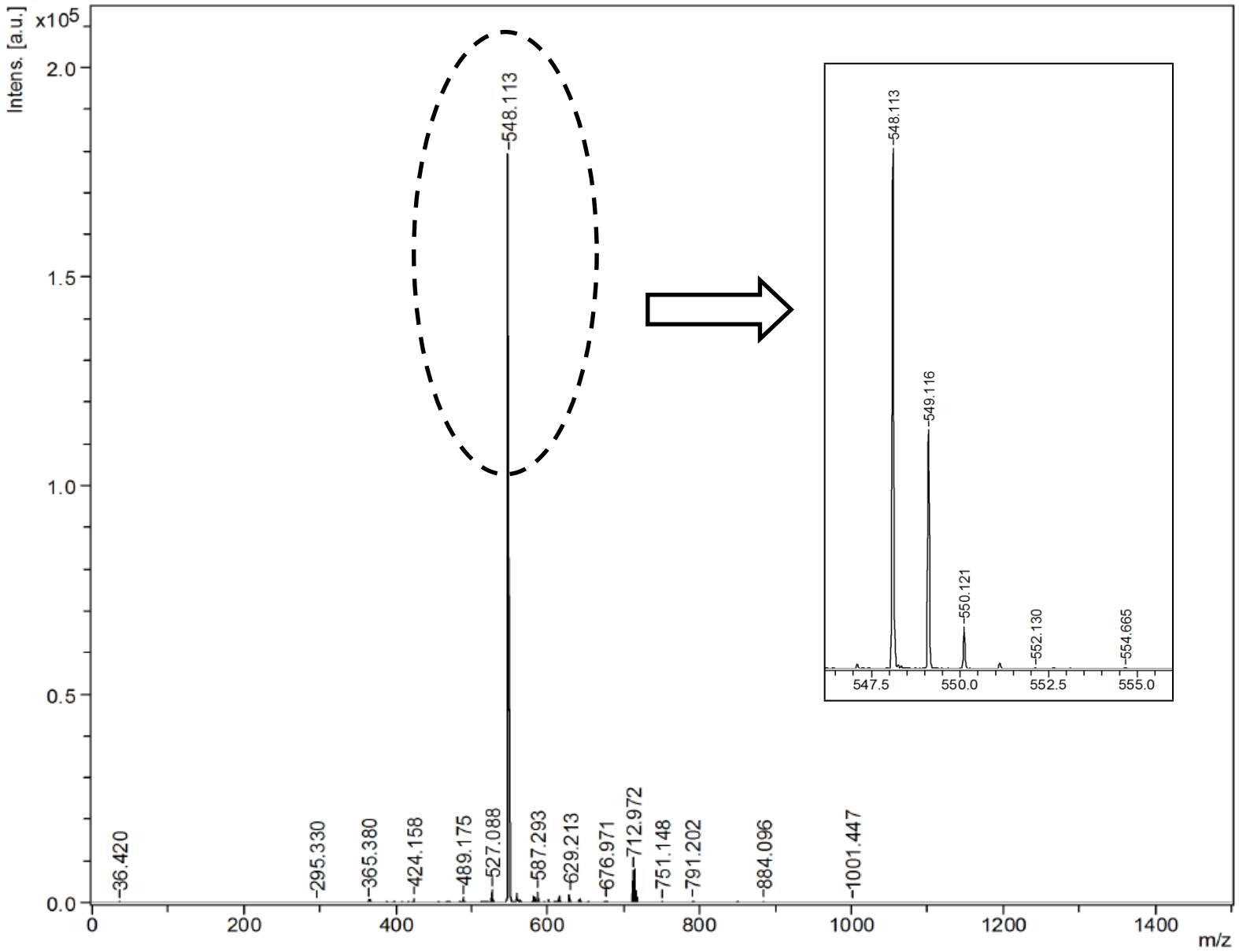

S13: MALDI of the complex formed with Ni^{2+} (Matrix DHB)

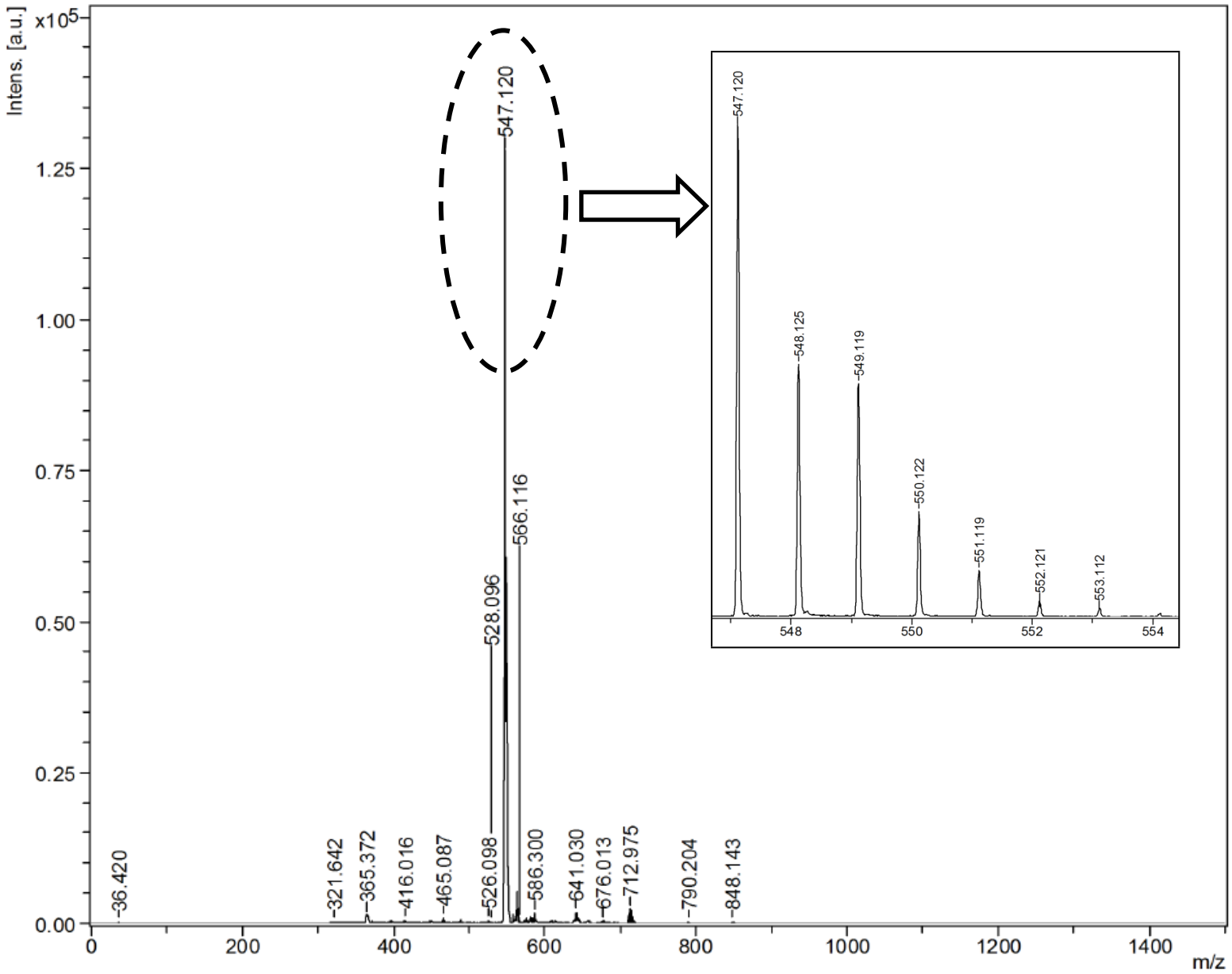

S14: MALDI of the complex formed with Cu^{2+} (Matrix DHB)

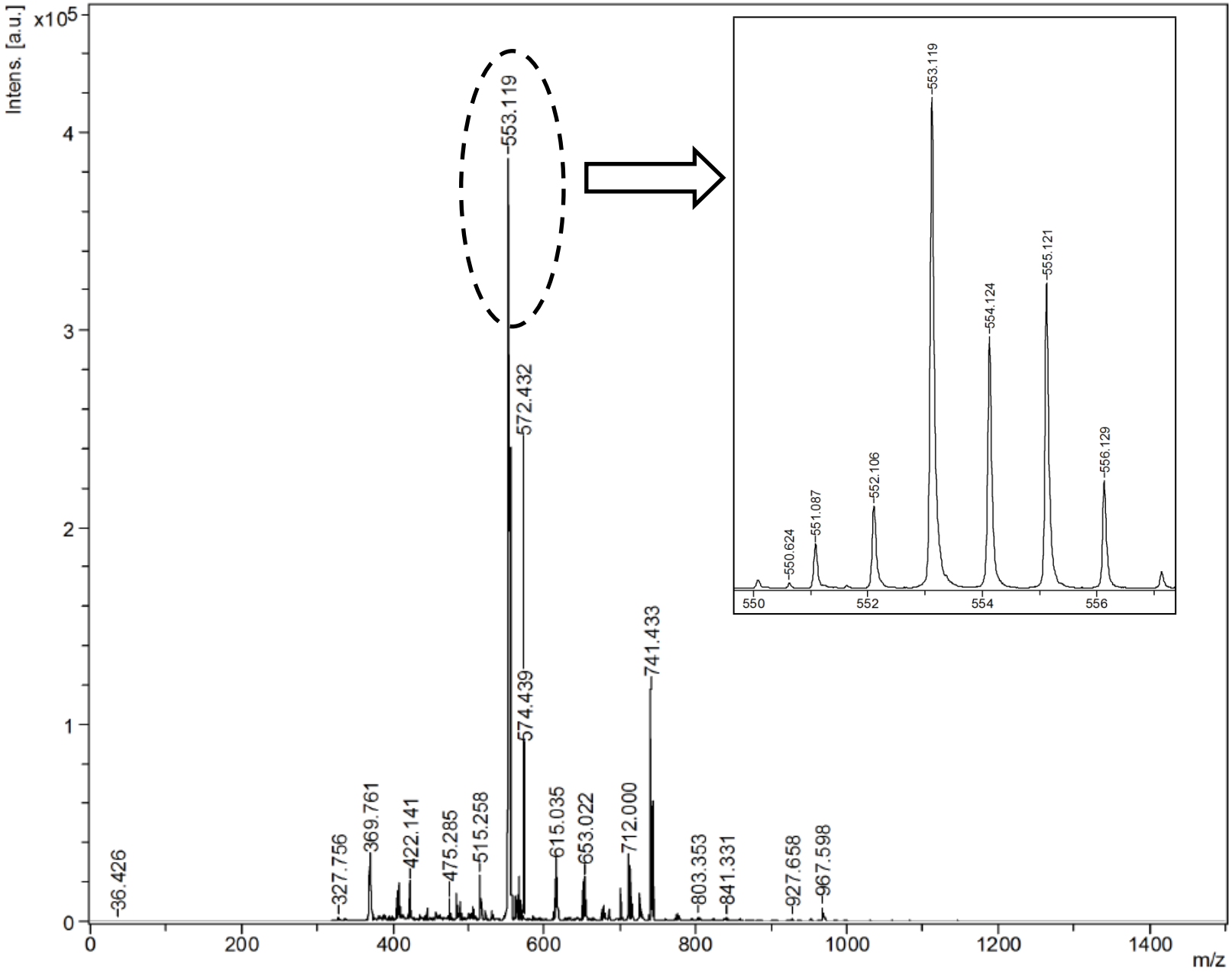

S15: UV-Visible spectra of PPQ with and without Zn^{2+} in DMF

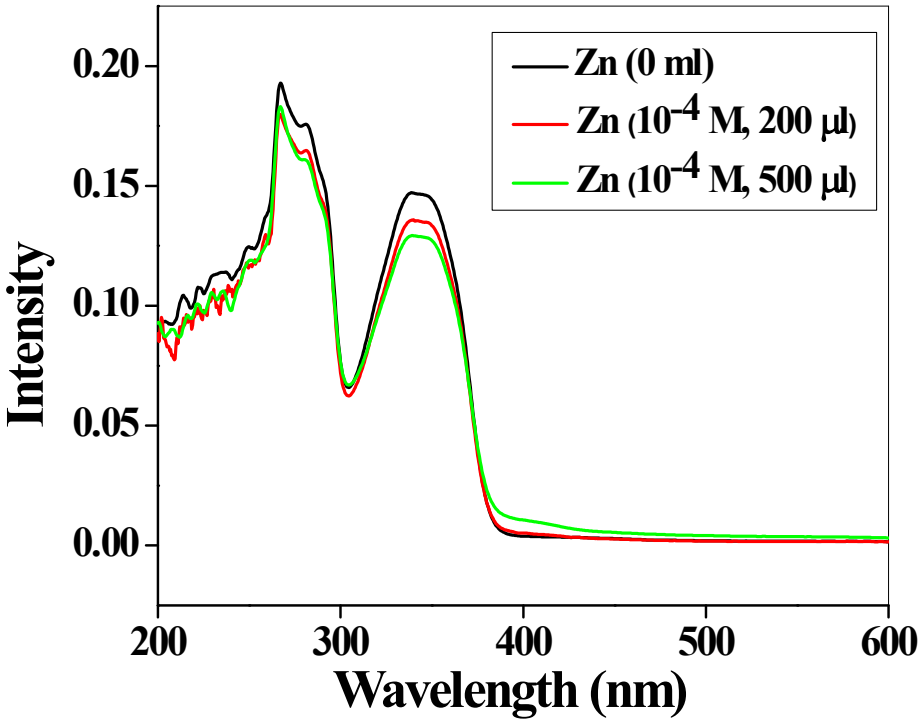

UV-Visible spectra of PPQ (10^{-5} M) with Zn^{2+} in DMF, λ_{max} is at 350 nm. However, we do not see any prominent change in the spectra after the addition of the metal, except the small decrease in intensity due to the dilution effect.

S16: TD DFT studies of PPQ and PPQ-Zn-PPQ

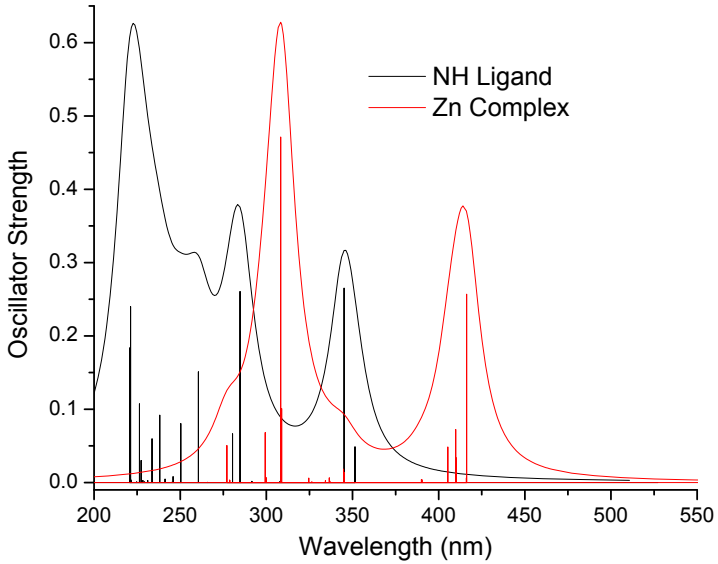

Figure 1R. *UV-Vis spectra ($S_0 \rightarrow S_n$, 1 <n< 26) of the NH ligand and Zn complex computed using time-dependent density functional theory. Vertical transition energies were computed from the fully optimized B3LYP/6-311++G** minima. The spectra are represented as sums of Lorentzians centered at the transition maxima (stick spectra), and individually broadened by 10 nm.*

Assuming Kasha's rule holds, fluorescence takes place from the lowest excited electronic state of a material system. The lowest lying excited electronic state in the NH ligand lies (vertically) at 351.47 nm (3.5276 eV) at the B3LYP/6-311++G** level of theory. Its analogue for promoting the Zn complex to S_1 - computed using the same level of theory - lies at 416.25 nm (2.9786 eV). The change in electron density associated with promoting the two systems to S_1 can be visualized in **Figures 2R and 3R**, shown below.

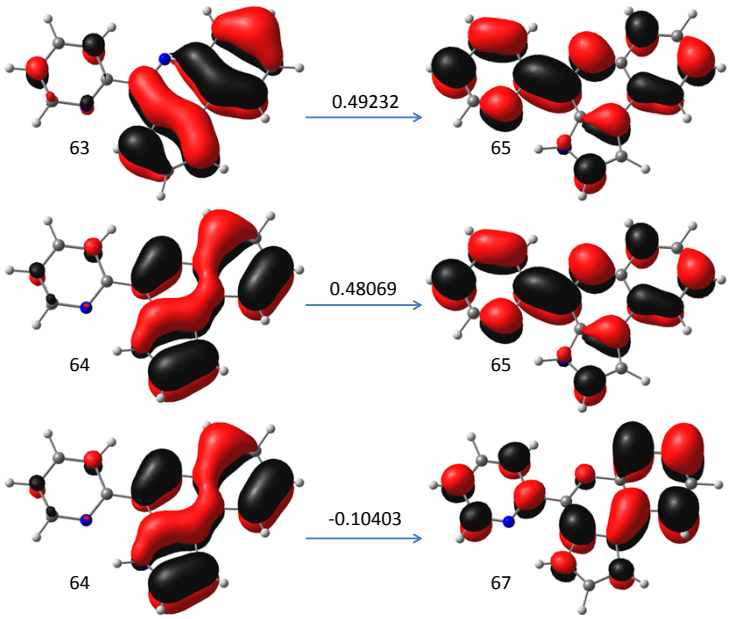

Figure 2R. *Change in electron density associated with $S_0 \rightarrow S_1$ excitation in the NH ligand. Orbital # 64 is the highest occupied molecular orbital (HOMO) in this system. The coefficients for the different excitations which contribute to the total transition are shown atop the individual arrows.*

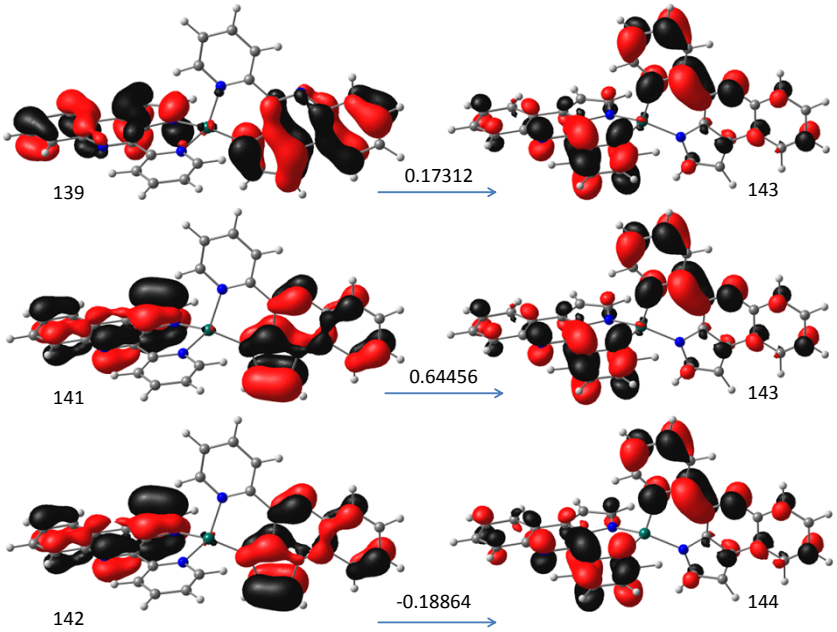

Figure 3R. *Change in electron density associated with $S_0 \rightarrow S_1$ excitation in the Zn complex. Orbital # 142 is the highest occupied molecular orbital (HOMO) in this complex. The coefficients for the different excitations which contribute to the total transition are noted atop the respective arrows.*

In this picture, for instance, one can notice that the change in electron density associated with $S_0 \rightarrow S_1$ excitation in the Zn complex do not involve the metal, and are mainly localized on the ligands. We find that the Frank-Condon arguments made above (and Kasha's picture) are perhaps adequate for qualitatively describing the photophysics in the NH ligand. Nonetheless, they fall short in describing the excited state processes in the complex, where rich photophysics seems to be at play, as we illustrate below.

We first recognize that fluorescence takes place from minima on the lowest excited electronic singlet state. This requires going beyond the above qualitative discussion, and necessitates geometry optimization on the excited electronic states of interest. Note that these are rather exhaustive simulations (especially for the Zn complex), as the frequency calculations - which are required to rigorously demonstrate that the geometry reached is indeed at a minimum - are carried out numerically in most electronic structure software packages we are aware of (including the G09 software which we employ in this work). This is why we opted to use the smaller 6-31g*

basis set in the ensuing calculations. The fully minimized S_0 and S_1 structures of the NH ligand are shown below. Note that we ensured that all the frequencies are positive in both cases.

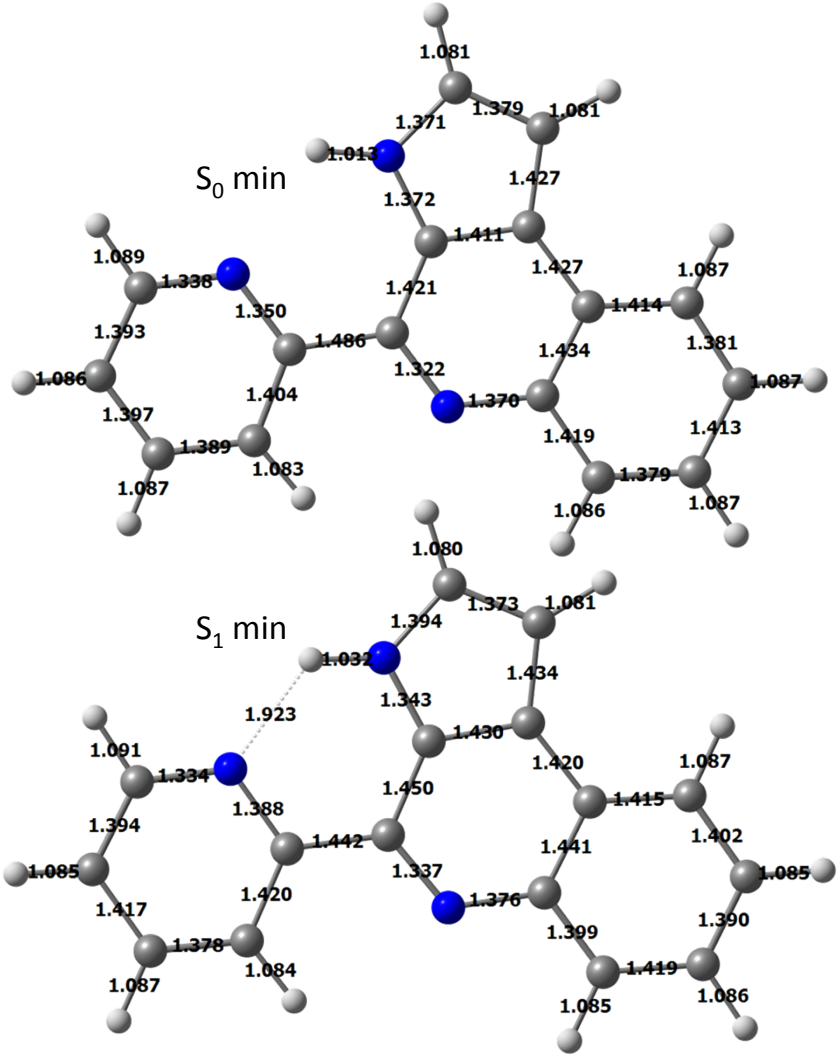

Figure 4R. *Optimized geometries of the NH ligand on S_0 and S_1 computed at the B3LYP/6-31g* level of theory.*

We then use the molecular structure corresponding to the fully relaxed S_1 geometry as a starting point for a single point energy calculation on S_0. The computed energy difference is 404.48 nm (3.065 eV), in excellent agreement with the measured fluorescence maximum of the NH ligand.

Similar calculations were performed in an attempt to describe the nature of fluorescent state in the complex. The structures are shown in **Figure 5R**.

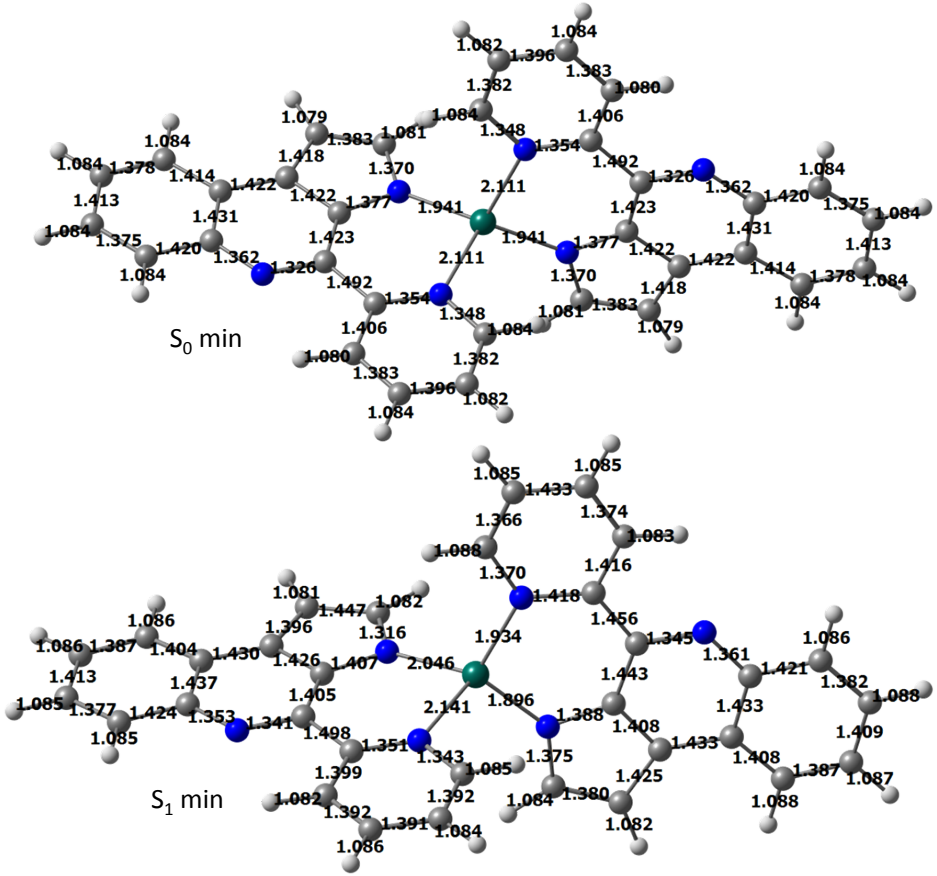

Figure 5R. *Optimized geometries of the Zn complex on S_0 and S_1 computed at the B3LYP/6-31g* level of theory.*

We again use the molecular structure corresponding to the fully relaxed S_1 geometry as a starting point for a single point energy calculation on S_0. The computed energy difference is 674.90 nm (1.837 eV), significantly red-shifted from the experimental value.

As violations to Kasha's rule have been documented in literature, we decided to explore the possibility that fluorescence is taking place from higher excited electronic states. Geometry optimization on S_2 yields the following structure:

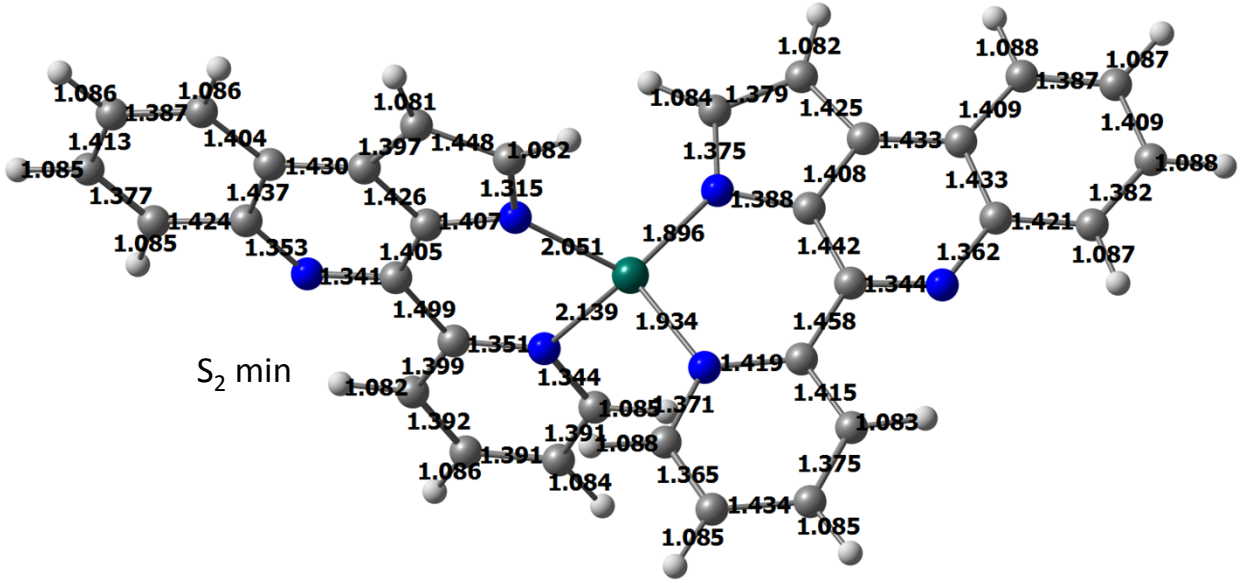

Figure 6R. *Optimized geometries of the Zn complex on S_2 computed at the B3LYP/6-31g* level of theory.*

Here, the surprising result was that the emission maximum from S_2 is predicted to lie at 696.51 nm (1.780 eV), 21.61 nm red-shifted from its S_1 analogue. We note that some 10 different starting structures were tested, and the system was found to exclusively relax to the same global minimum on S_2, shown in **Figure 6R**.

Possible interpretation of these results:

It is possible that the level of theory employed, although properly describing the excited state properties NH ligand, is not adequate for the complex. For instance, surface crossings - which are abundant in organics and organometallics – may be playing a role in steering the excited state species from the Frank-Condon regions to the minima on S_2 and S_1. The yielded energetics are suggestive of the aforementioned, and tools of TD DFT are known to miss out on the proper dimensionality of the beyond Born-Oppenheimner problem. Another possibility is that the solvent plays an intimate role in the photophysics of the complex (some explicit solute-solvent interaction), one which is naturally not captured by the gas phase model employed.

All in all, we find that rigorously assigning the recorded fluorescence maximum of the complex is not a trivial task at present. This would require a full theoretical investigation, one which goes far beyond the scope of the present work. It is a challenge that we will attempt to take on in follow-up reports.

References

1. Schwalm CS, Correia CRD (2012) Tetrahedron Lett 53:4836.
2. Akula M, Sridevi, JP, Yogeeswari P, Sriram D, Bhattacharya A (2014) Monat. Chemie. 145:811.